

Automatika

Journal for Control, Measurement, Electronics, Computing and Communications



ISSN: (Print) (Online) Journal homepage: <https://www.tandfonline.com/loi/taut20>

Noise and sensitivity comparison for different BP filter designs

Zoran Šverko, Nino Stojković, Saša Vlahinić & Ivan Markovinović

To cite this article: Zoran Šverko, Nino Stojković, Saša Vlahinić & Ivan Markovinović (2021) Noise and sensitivity comparison for different BP filter designs, *Automatika*, 62:3-4, 319-330, DOI: 10.1080/00051144.2021.1949532

To link to this article: <https://doi.org/10.1080/00051144.2021.1949532>



© 2021 The Author(s). Published by Informa UK Limited, trading as Taylor & Francis Group.



Published online: 06 Jul 2021.



Submit your article to this journal [↗](#)



Article views: 643



View related articles [↗](#)



View Crossmark data [↗](#)



Noise and sensitivity comparison for different BP filter designs

Zoran Šverko , Nino Stojković, Saša Vlahinić and Ivan Markovinović

Faculty of Engineering, Department of Automatics and Electronics, University of Rijeka, Rijeka, Croatia

ABSTRACT

In this paper, the analysis of noise and sensitivity for different BP filter designs is observed. Calculation of the voltage noise spectral density, root mean square (RMS) value of the noise voltage, Schoeffler sensitivity and the multi-parameter sensitivity is done for the simply designed (SD) active RC, noise and sensitivity optimized (NO and SO) active RC, operational transconductance amplifiers (OTA-C) and switched capacitor (SC) filter designs. This is observed for the fourth-order Chebyshev band-pass filter, with central frequency $f_c = 4$ kHz, bandwidth 1 kHz and pass-band ripple $\alpha_{\max} = -0.1$ dB. Cascade of two second-order sections is used for fulfilment realization of all four observing designs. Programming tools, such as MATLAB and SPICE (LTspice), are also used for the analyses.

Highlights

- We used three different designs and optimization (noise and sensitivity) procedure for design and optimize the fourth-order Chebyshev band-pass filter
- Our results suggest which design is best to use for improving noise and sensitivity of this filter
- MATLAB and SPICE software were used for calculations and simulations of different band-pass filter designs and analysis of noise and sensitivity

ARTICLE HISTORY

Received 13 May 2020
Accepted 15 June 2021

KEYWORDS

Band-pass filter; noise; sensitivity; SC filter; design

1. Introduction

In practice, we have different ways to realize the same transfer function of the filter. The most frequently used realization is the one with operational amplifiers (OA). The OA realization provides a continuous-time output voltage as well as low output impedance. Furthermore, the realization with the general transconductance amplifier (OTA-C) is used for the purpose of the high impedance output. Moreover, the realization with switched capacitors (SC) is another frequently used type of the realization of the same filter transfer function [1–3]. The SC realization of filter is suitable for monolithic integrated technology conception. In this conception, the filter is entirely made in a chip using the thick and thin film technology.

During the design of the filter, we usually need to fulfil specifications on amplitude and phase filter characteristics. Furthermore, some other additional parameters of quality filter design can be observed. Some of them are noise and sensitivity. The main goal is to reduce noise and sensitivity to the maximum extent possible, because the important transmitted information can be covered with the superposition of noise on the main signal. On the other hand, sensitivity shows

us a change in amplitude and in phase filter characteristics during the change element values of a filter. This is important because of the decision to choose appropriate tolerance of elements for the application of a filter. In this paper, designs, based on OA, OTA-C and SC realization techniques to reduce noise [4] and sensitivity [5,6] in a filter, will be shown. This paper is an extension of the conference paper [4].

2. Realization

For our research, we used Chebyshev band-pass filter with the normed transfer function shown in the below equations [4]:

$$H(s) = H_1(s) \cdot H_2(s) \quad (1a)$$

$$H_1(s) = \frac{0.4525s}{s^2 + 0.2456s + 0.7066} \quad (1b)$$

$$H_2(s) = \frac{0.4525s}{s^2 + 0.3475s + 1.415} \quad (1c)$$

$$H(s) = \frac{0.2048s^2}{s^4 + 0.5931s^3 + 2.207s^2 + 0.5931s + 1} \quad (1d)$$

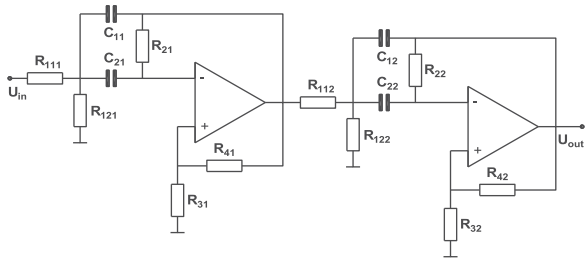


Figure 1. Fourth-order OA band-pass filter [4].

Chebyshev band-pass filter is denormed on a frequency of 4 kHz. The transfer functions of the fourth-order denormed Chebyshev band-pass filter and its sections are shown below [4]:

$$H(s) = H_1(s) \cdot H_2(s) \quad (2a)$$

$$H_1(s) = \frac{-5.3542 \cdot 10^3 s}{s^2 + 4.1764 \cdot 10^3 s + 7.5469 \cdot 10^8} \quad (2b)$$

$$H_2(s) = \frac{-6.3969 \cdot 10^3 s}{s^2 + 3.4956 \cdot 10^3 s + 5.2869 \cdot 10^8} \quad (2c)$$

$$H(s) = \frac{3.4251 \cdot 10^7 s^2}{s^4 + 7.672 \cdot 10^3 s^3 + 1.2979 \cdot 10^9 s^2 + 4.8462 \cdot 10^{12} s + 3.99 \cdot 10^{17}} \quad (2d)$$

2.1. Continuous-time active RC filters

The Single Amplifier Biquad (SAB) topology of the band-pass filter is shown in Figure 1.

The cascade of two second-order sections is used for realization. The transfer function of the circuit [4] is shown as

$$H(s) = \prod_{i=1,2} H_i(s) \quad (3a)$$

$$H_i(s) = \frac{-\left(1 + \frac{G_{4i}}{G_{3i}}\right) \frac{G_{11i} s}{C_{1i}}}{s^2 + s \left(\frac{G_{2i}}{C_{1i}} + \frac{G_{2i}}{C_{2i}} - \frac{G_{1i} G_{4i}}{C_{1i} G_{3i}} \right) + \frac{G_{1i} G_{2i}}{C_{1i} C_{2i}}} \quad (3b)$$

Element values can be calculated using manipulation and comparison of Equations (2a) to (2c) with (3a) and (3b), where $C_{1i} = C_{2i}$ and $R_{1i} = R_{2i}$. Values in Table 1 are taken from [7].

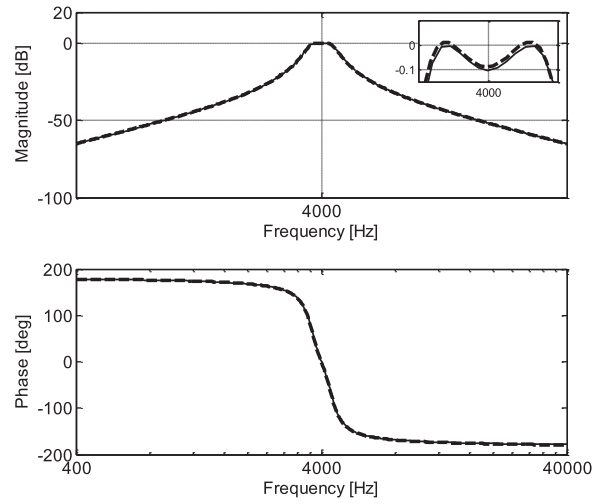


Figure 2. Frequency response of the fourth-order continuous-time active-RC SD [4].

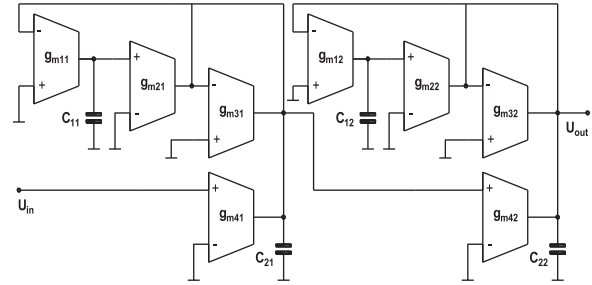


Figure 3. Fourth-order OTA-C band-pass filter [4].

Frequency responses of the filter are shown in Figure 2. Using a simulating circuit, shown in Figure 1 and element values from Table 1, simulated values of the frequency response are shown. The frequency response of the calculated values is given using filter transfer function (2a) to (2c). A marginal difference between simulated (dashed) and calculated (solid) characteristics can be seen in the zoomed inset of Figure 2.

2.2. OTA-C filter

The cascade of two second-order general transconductance amplifier sections [8] is used for realization, as shown in Figure 3.

Table 1. Element values of simply designed (SD), noise optimized (NO) and sensitivity optimized (SO) continuous active-RC filters [7].

	SD		NO		SO	
	1st section	2nd section	1st section	2nd section	1st section	2nd section
R_{11i}	53.1915 k Ω	44.5208 k Ω	21.3238 k Ω	21.3238 k Ω	17.9569 k Ω	17.9569 k Ω
R_{12i}	3.9075 k Ω	4.81995 k Ω	1.5299 k Ω	1.8538 k Ω	0.7667 k Ω	0.9238 k Ω
R_{2i}	3.6401 k Ω	4.3491 k Ω	9.2824 k Ω	11.0902 k Ω	18.0187 k Ω	21.5280 k Ω
R_{3i}	7.3529 k Ω	7.35294 k Ω	0.9866 k Ω	0.9866 k Ω	0.2025 k Ω	0.2025 k Ω
R_{4i}	3.9789 k Ω					
C_{1i}	10 nF					
C_{2i}	10 nF					
k_j	1	1	2.55	2.55	4.95	4.95

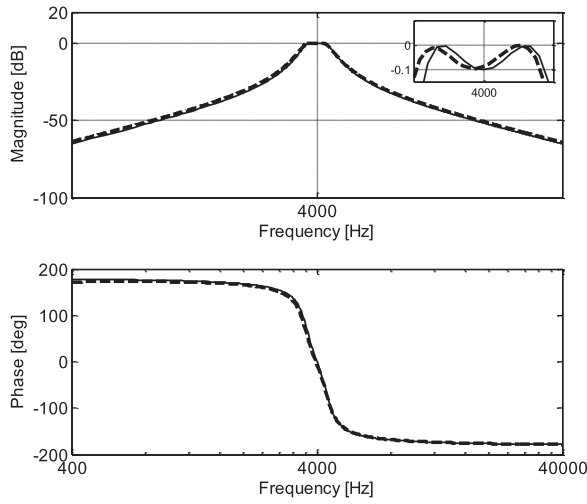


Figure 4. Frequency response of the fourth-order OTA-C band-pass filter [4].

Table 2. Element values of OTA-C filter.

	1st section	2nd section
g_{m1i}	2.7472 mS	2.2993 mS
g_{m2i}	2.7472 mS	2.2993 mS
g_{m3i}	0.41764 mS	0.34956 mS
g_{m4i}	0.53542 mS	0.63969 mS
C_{1i}	100 nF	100 nF
C_{2i}	100 nF	100 nF

The transfer function of the circuit is shown as

$$H(s) = \prod_{i=1,2} H_i(s) \quad (4a)$$

$$H_i(s) = \frac{\left(\frac{g_{m4i}}{C_{2i}}\right) s}{s^2 + s\left(\frac{g_{m3i}}{C_{2i}}\right) + \left(\frac{g_{m1i}g_{m2i}}{C_{1i}C_{2i}}\right)} \quad (4b)$$

Element values of the OTA-C filter were calculated using a comparison of Equations (4a), (4b) with (2a)–(2c). These element values are shown in Table 2. Figure 4 shows frequency responses of the OTA-C filter.

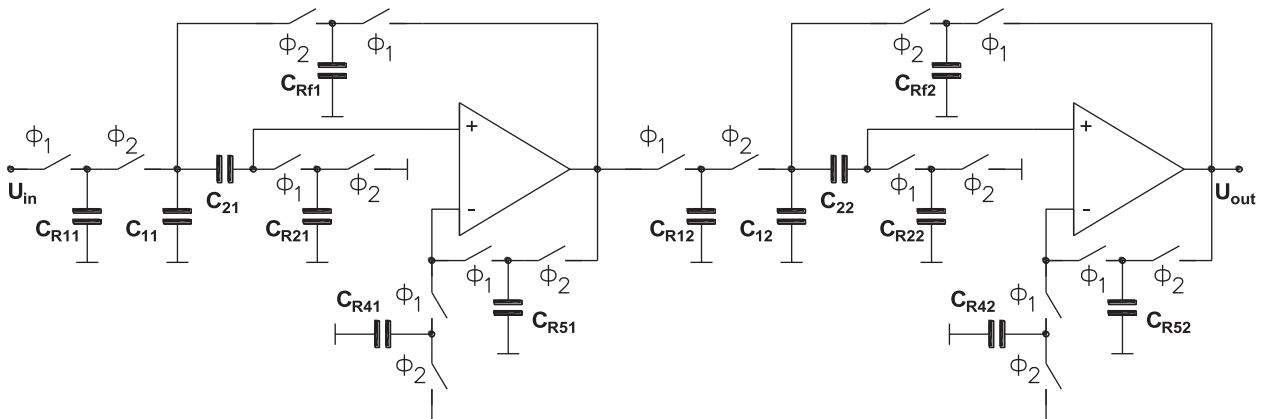


Figure 5. Fourth-order SC band-pass filter (SAK topology) [4].

2.3. Discrete time SC filter

Figure 5 explains the discrete time SC filter based on the Sallen-Key (SAK) topology [9].

The forward Euler transformation ($s \rightarrow (z-1)/T_s$) has been implemented for the calculation of the discrete transfer function [10]. The sampling time T_s has been calculated as $T_s = 1/f_s$ where $f_s = 4900f_c$.

$$H(z) = H_1(z) \cdot H_2(z) \quad (5a)$$

$$H_1(z) = \frac{5.8023 \cdot 10^{-4} \cdot (z-1)}{z^2 - 1.9997z + 0.9997} \quad (5b)$$

$$H_2(z) = \frac{5.8023 \cdot 10^{-4} \cdot (z-1)}{z^2 - 1.9996z + 0.9996} \quad (5c)$$

$$H(z) = \frac{3.3667 \cdot 10^{-7} (z^2 - 2z + 1)}{z^4 - 3.9992z^3 + 5.9977z^2 - 3.9977z + 0.9992} \quad (5d)$$

The discrete transfer function of SC filter built on the Sallen-Key topology is given by [4]

$$H(z) = \prod_{i=1,2} G_i \cdot \frac{a_{1i} \cdot (z-1)}{a_{2i} \cdot z^2 - a_{3i} \cdot z + a_{4i}} \quad (6a)$$

$$G_i = 1 + C_{4i}/C_{5i} \quad (6b)$$

$$a_{1i} = C_{1i}C_{2i}C_{R1i} \quad (6c)$$

$$a_{2i} = C_{1i}^2C_{2i} + C_{1i}C_{2i}C_{R1i} + C_{1i}^2C_{R2i} + C_{1i}C_{2i}C_{R2i} + C_{1i}C_{R1i}C_{R2i} + C_{2i}C_{R1i}C_{R2i} + C_{1i}C_{2i}C_{Rfi} + C_{1i}C_{R2i}C_{Rfi} + C_{2i}C_{R2i}C_{Rfi} \quad (6d)$$

$$a_{3i} = 2C_{1i}^2C_{2i} + C_{1i}C_{2i}C_{R1i} + C_{1i}^2C_{R2i} + C_{1i}C_{2i}C_{R2i} + C_{2i}C_{R1i}C_{R2i} + C_{1i}C_{2i}C_{Rfi} + C_{2i}C_{R2i}C_{Rfi} + G_iC_{1i}C_{2i}C_{Rfi} \quad (6e)$$

$$a_{4i} = C_{1i}^2C_{2i} + G_iC_{1i}C_{2i}C_{Rf} \quad (6f)$$

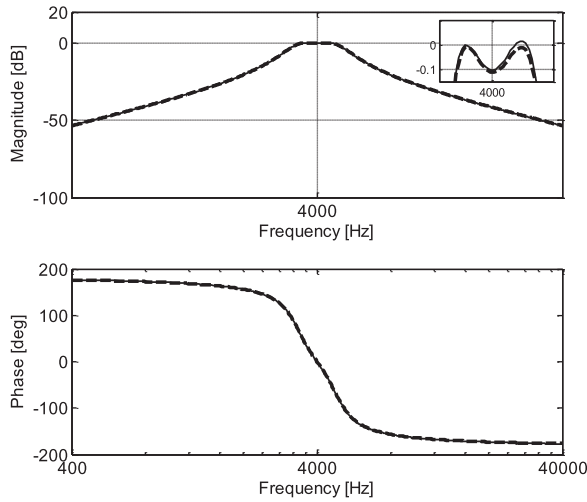


Figure 6. Frequency response of the fourth-order SC band-pass filter [4].

Table 3. Element values of SC filter [4].

	1st section	2nd section
C_{R1i}	37.9 pF	53.7 pF
C_{R2i}	2.82 pF	2.52 pF
C_{1i}	120 nF	120 nF
C_{2i}	3.3 nF	3.3 nF
C_{Rfi}	125.5 pF	313.5 pF
C_{4i}	2.15 nF	1.53 nF
C_{5i}	2.55 nF	5.1 nF

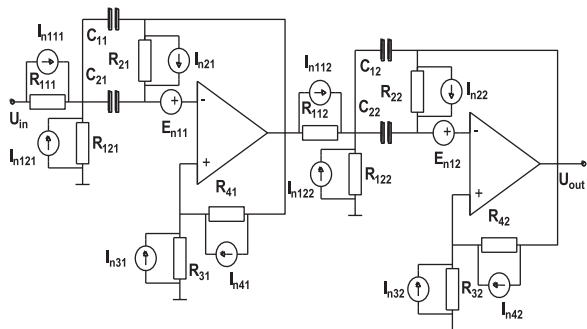


Figure 7. Equivalent electrical noise circuit of the fourth-order SD and NO band-pass filter [4].

Element values were calculated using a comparison of Equations (5a)–(5c) with (6a)–(6f). Element values of the SC filter are outlined in Table 3.

When comparing Figure 6 with Figure 2, we can establish that Z-transformation has no unwanted impacts on filter specifications.

3. Noise

3.1. Noise in filter with OA

An equivalent circuit of the active-RC filter for the calculation of the voltage noise spectral density is shown in Figure 7.

Current noise sources: $I_{ni} = \sqrt{4kT/R_i}$ have been inserted parallel to the resistors. Moreover, voltage

noise sources $E_n = 2.5 \text{ nV}/\sqrt{\text{Hz}}$ (for LT1007) have been inserted at the input of the operational amplifier. The value of the input current noise source ($I_n = 0.4 \text{ pA}/\sqrt{\text{Hz}}$) of the operational amplifier is much lower than that the voltage noise source, and was therefore neglected.

Equation (7) was used for the calculation of the voltage noise spectral density [11]:

$$V_n^2(\omega) = \sum^m |T_{I,k}(j\omega)|^2 (I_{n,k})^2 + \sum^n |T_{V,i}(j\omega)|^2 (E_{n,i})^2 \quad (7)$$

In Equation (7), the transfer functions of the voltage noise sources $E_{n,i}$ and the current noise sources $I_{n,i}$ are denoted by $T_{V,i}$ and $T_{I,k}$, respectively. Total voltage noise spectral density and noise components for both sections are shown in Figure 8.

Using theoretical values based on thermal noise sources in calculations and real elements noise models using SPICE, we can see the difference between calculated and simulated values. Equation (8) shows a calculation for the RMS value:

$$(E_n^2)_{ef} = \int_{\omega_1}^{\omega_2} V_n^2(\omega) d\omega \quad (8)$$

We used the optimization algorithm given in [7] because we wanted to reduce voltage noise spectral density of the filter. For decreasing noise results, all element values were taken from [7], recalculated and tested in MATLAB and SPICE. Figure 9(a) shows the total voltage noise spectral density of NO filter design, while noise components are specified in Figure 9(b,c) for both sections.

We can conclude that the noise-optimized filters (NO) produce a smaller RMS noise value than the non-noise-optimized filters (SD).

3.2. Noise in OTA-C filter

Figure 10 shows the equivalent circuit for the calculation of the voltage noise spectral density of the observed OTA-C filter.

Voltage noise spectral density is calculated using Equation (7). Figure 11 shows the total voltage noise spectral density. Using theoretical values based on thermal noise sources in calculations by MATLAB and real elements noise models by SPICE, we can ascertain the distinction between calculated and simulated values. The noise components for both sections are shown in Figure 11(b,c). In this design, LT1228 was used as a transconductance amplifier. The mentioned transconductance amplifier has the input voltage noise source of $E_n = 6 \text{ nV}/\sqrt{\text{Hz}}$ and the input current noise source $I_n = 1.4 \text{ pA}/\sqrt{\text{Hz}}$. Considering these facts, the current noise source is much lower than the voltage noise source, and for this reason it was neglected in the calculation.

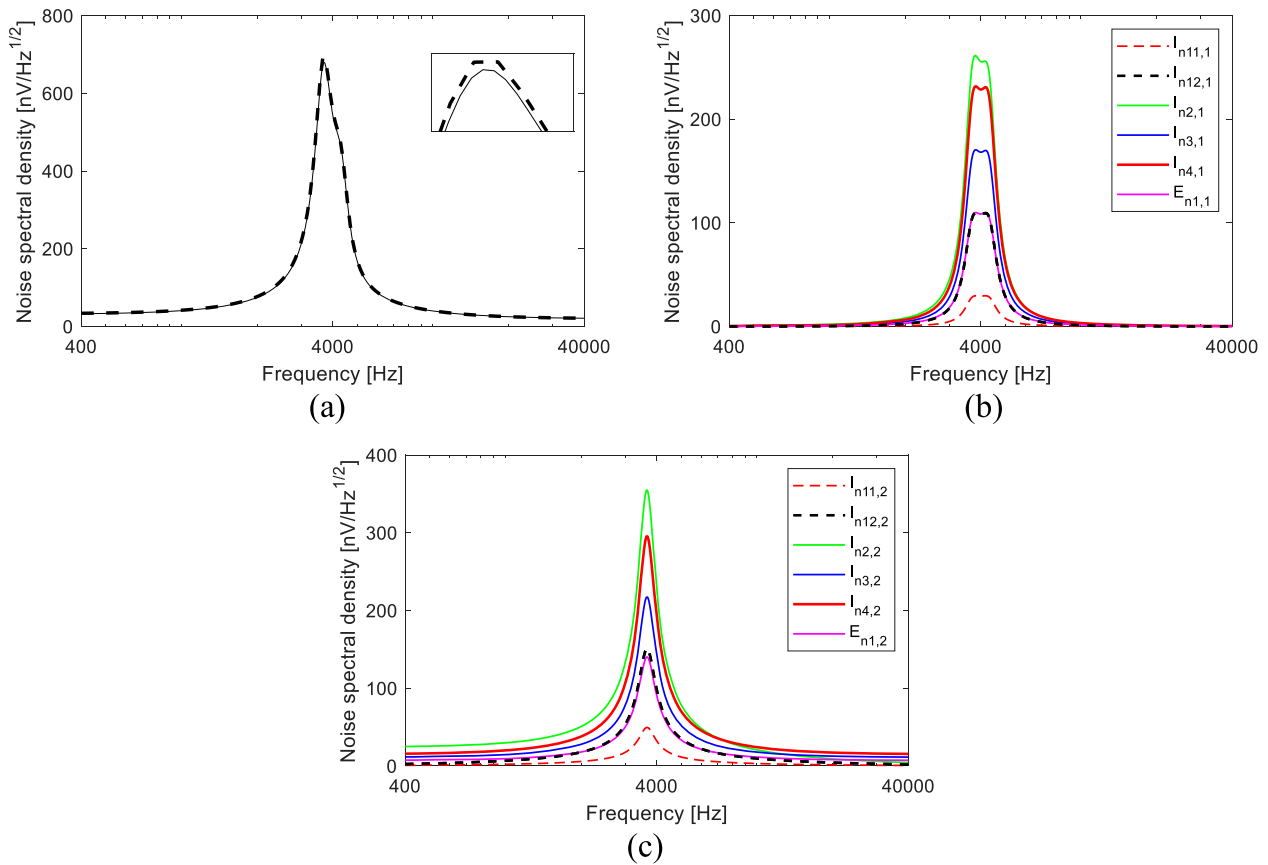


Figure 8. Noise voltage spectral density of the fourth-order SD band-pass filter and its components. (a) Total noise voltage spectral density: simulated (dashed) and calculated (solid). Noise RMS value is $E_n = 54.556 \mu\text{V}$. (b) Section 1 noise voltage spectral density components. Noise RMS value is $E_n = 34.805 \mu\text{V}$. (c) Section 2 noise voltage spectral density components. Noise RMS value is $E_n = 42.011 \mu\text{V}$ [4].

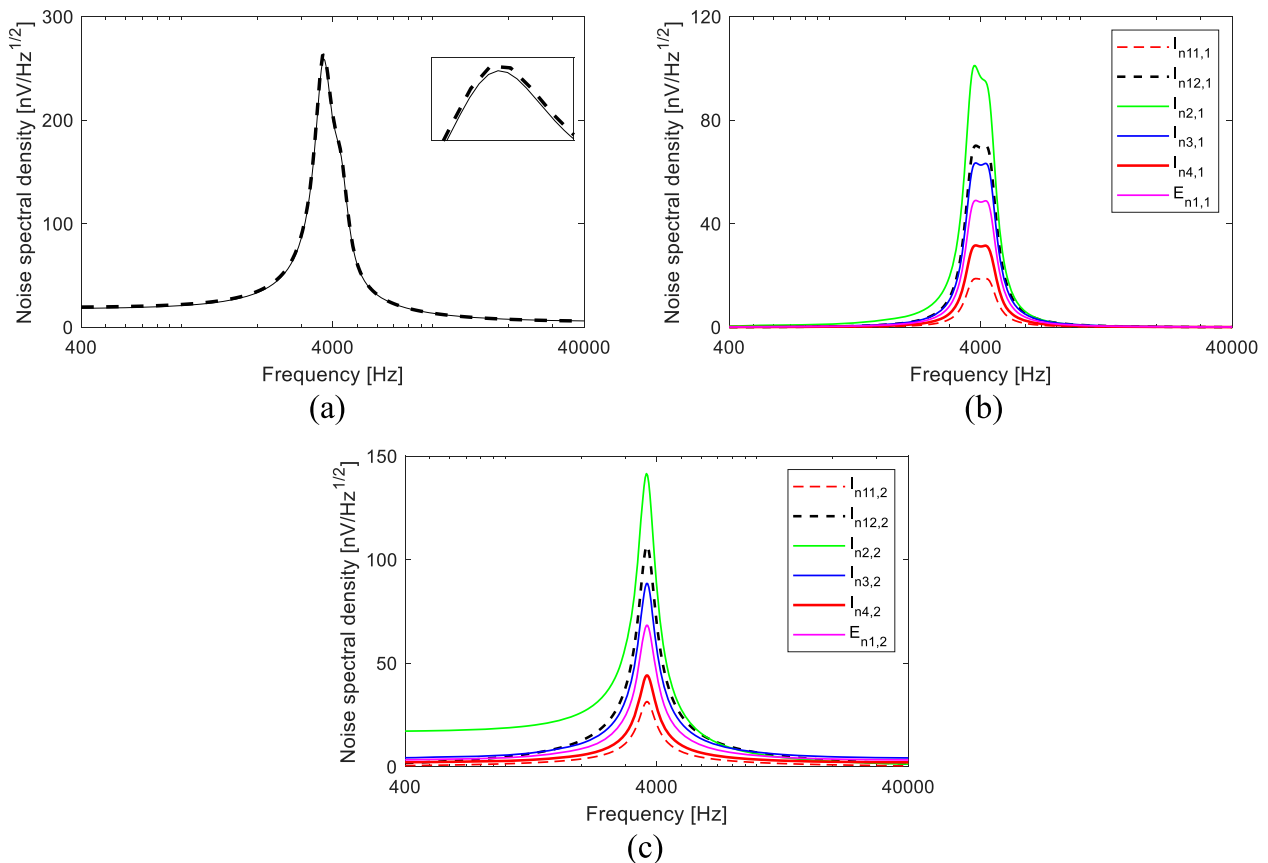


Figure 9. Noise voltage spectral density of the fourth-order NO band-pass filter and its components. (a) Total noise voltage spectral density: simulated (dashed) and calculated (solid). Noise RMS value is $E_n = 20.412 \mu\text{V}$. (b) Section 1 noise voltage spectral density components. Noise RMS value is $E_n = 12.422 \mu\text{V}$. (c) Section 2 noise voltage spectral density components. Noise RMS value is $E_n = 16.197 \mu\text{V}$. [4].

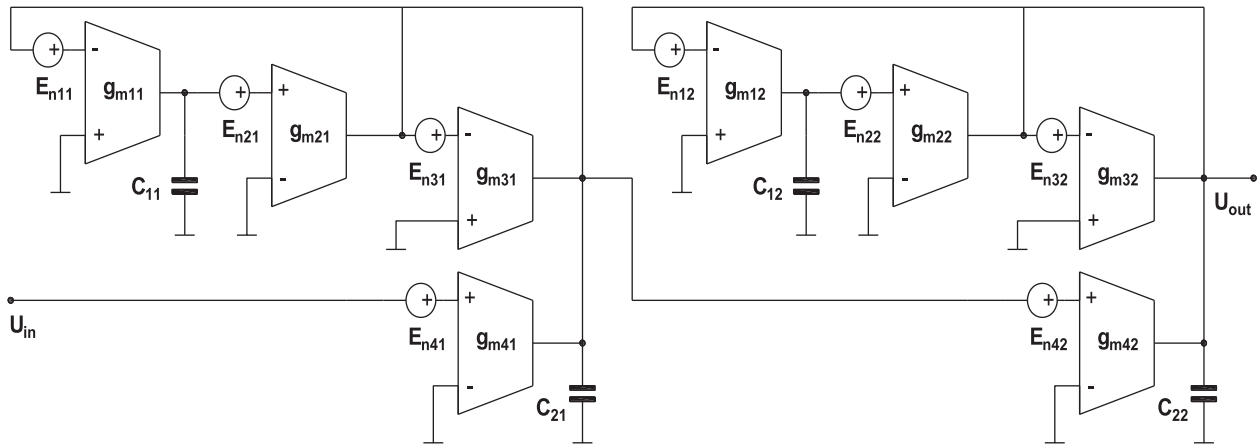


Figure 10. Equivalent electrical noise circuit of the fourth-order OTA-C band-pass filter [4].

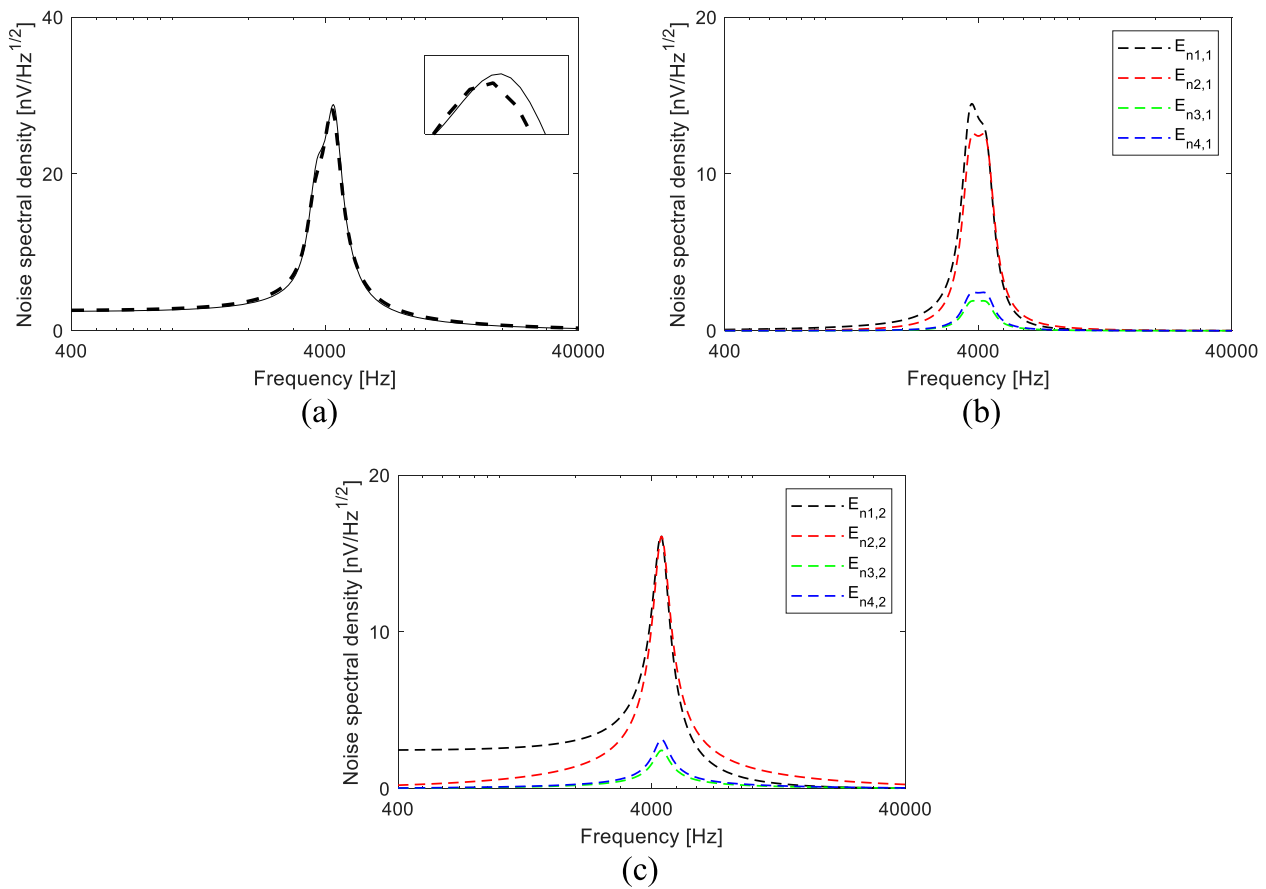


Figure 11. Noise voltage spectral density of the fourth-order OTA-C band-pass filter and its components. (a) Total noise voltage spectral density: simulated (dashed) and calculated (solid). Noise RMS value is $E_n = 2.4384 \mu\text{V}$. (b) Section 1 noise voltage spectral density components. Noise RMS value is $E_n = 1.5715 \mu\text{V}$. (c) Section 2 noise voltage spectral density components. Noise RMS value is $E_n = 1.8645 \mu\text{V}$. [4].

3.3. Noise in SC filter

Figure 5 shows the fourth-order SC band-pass filter. The calculation of voltage noise spectral density [12] of the equivalent circuit was based on [13]. The total voltage noise spectral density and its components are shown in Figure 12.

3.4. Noise comparison

Table 4 shows the RMS voltage noise value as the indicator of noise reduction.

This value is measured between $0.1f_c$ and $10f_c$, where f_c is the centre frequency of the band-pass filter. The voltage noise spectral density, for all filter designs studied in this paper, is shown in Figure 13.

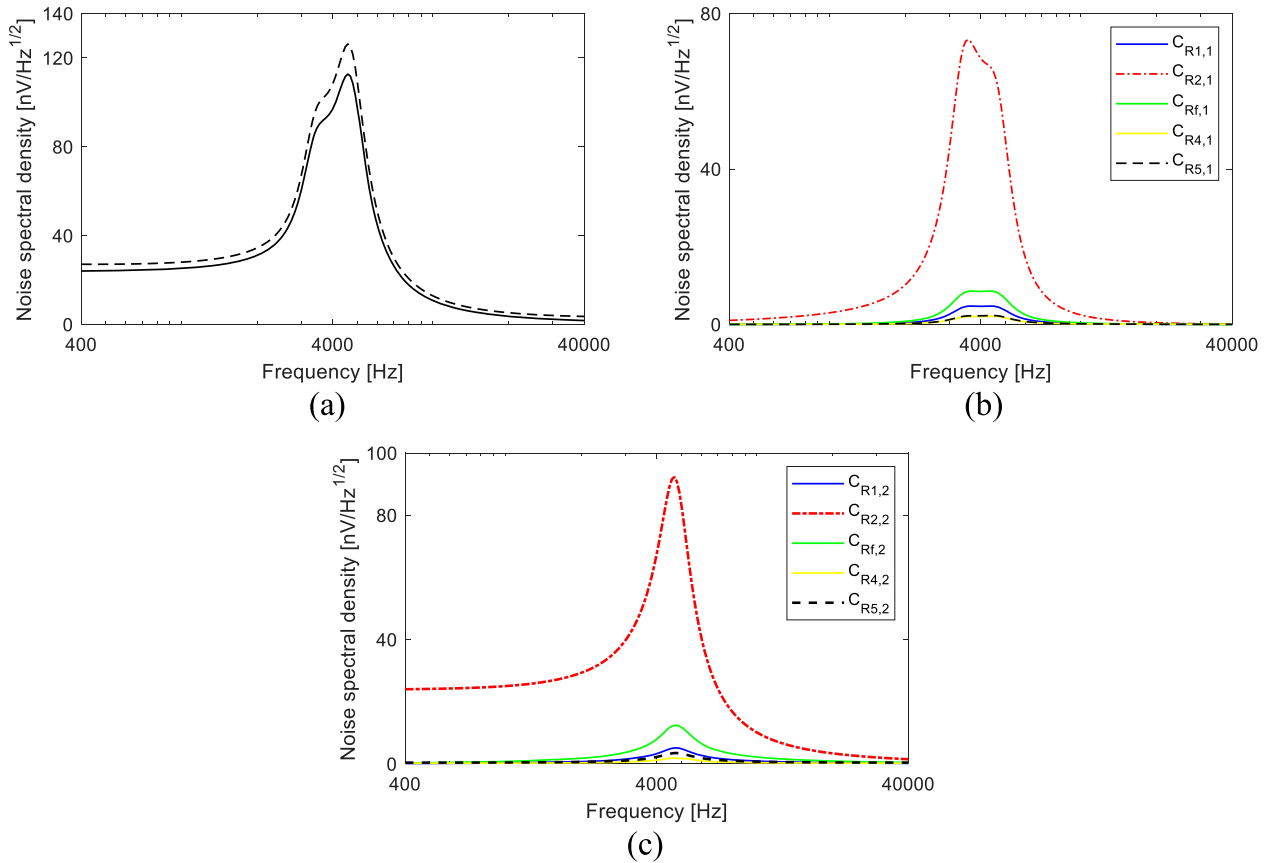


Figure 12. Noise voltage spectral density of the fourth-order discrete time SC band-pass filter and its components. (a) Total noise voltage spectral density: simulated (dashed) and calculated (solid). Noise RMS value is $E_n = 5.3954 \mu\text{V}$. (b) Section 1 noise voltage spectral density components. Noise RMS value is $E_n = 3.2451 \mu\text{V}$. (c) Section 2 noise voltage spectral density components. Noise RMS value is $E_n = 4.3022 \mu\text{V}$. [4].

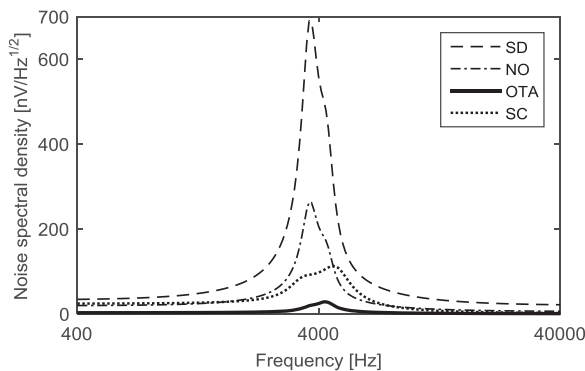


Figure 13. Noise voltage spectral density for: SD (dashed), NO (dashed-dot), OTA-C (solid), SC (dot-dot) [4].

Table 4. Noise RMS value comparison [4].

	SD	NO	OTA-C	SC
E_n	54.556 μV	20.412 μV	2.4384 μV	5.3954 μV

4. Sensitivity

4.1. Sensitivity in a filter with OA

A method for analysing sensitivity is described in [14]. Sensitivity analysis can be specified as the impact of the deviation of passive element values x_i on the filter

amplitude response characteristic $|H(j\omega)|$. The Schoeffler sensitivity was calculated using Equation (9), taken from [14]:

$$I_s^2(\omega) = \sum_i (S_{x_i}^{|H(j\omega)|})^2 \quad (9)$$

where

$$S_{x_i}^{|H(j\omega)|} = \frac{d|H(j\omega)|}{dx_i} \cdot \frac{x_i}{|H(j\omega)|} \quad (11)$$

For the comparison of the results, the multi-parameter sensitivity was calculated by Equation (11):

$$M = \int_{\omega_1}^{\omega_2} I_s^2(\omega) d\omega \quad (11)$$

Furthermore, the simulation of filter sensitivity was done using SPICE software for the Monte Carlo analysis. This analysis has been run over 100 passes with $\pm 1\%$ element tolerance.

The total Schoeffler sensitivity of the fourth-order SD band-pass filter is given in Figure 14(a). Moreover, Figure 14(b,c) shows the Schoeffler sensitivity components for both filter sections. These values were calculated with MATLAB.

By monitoring Figure 14, we can conclude that the sensitivity of R_{2i} element in both sections has strongest

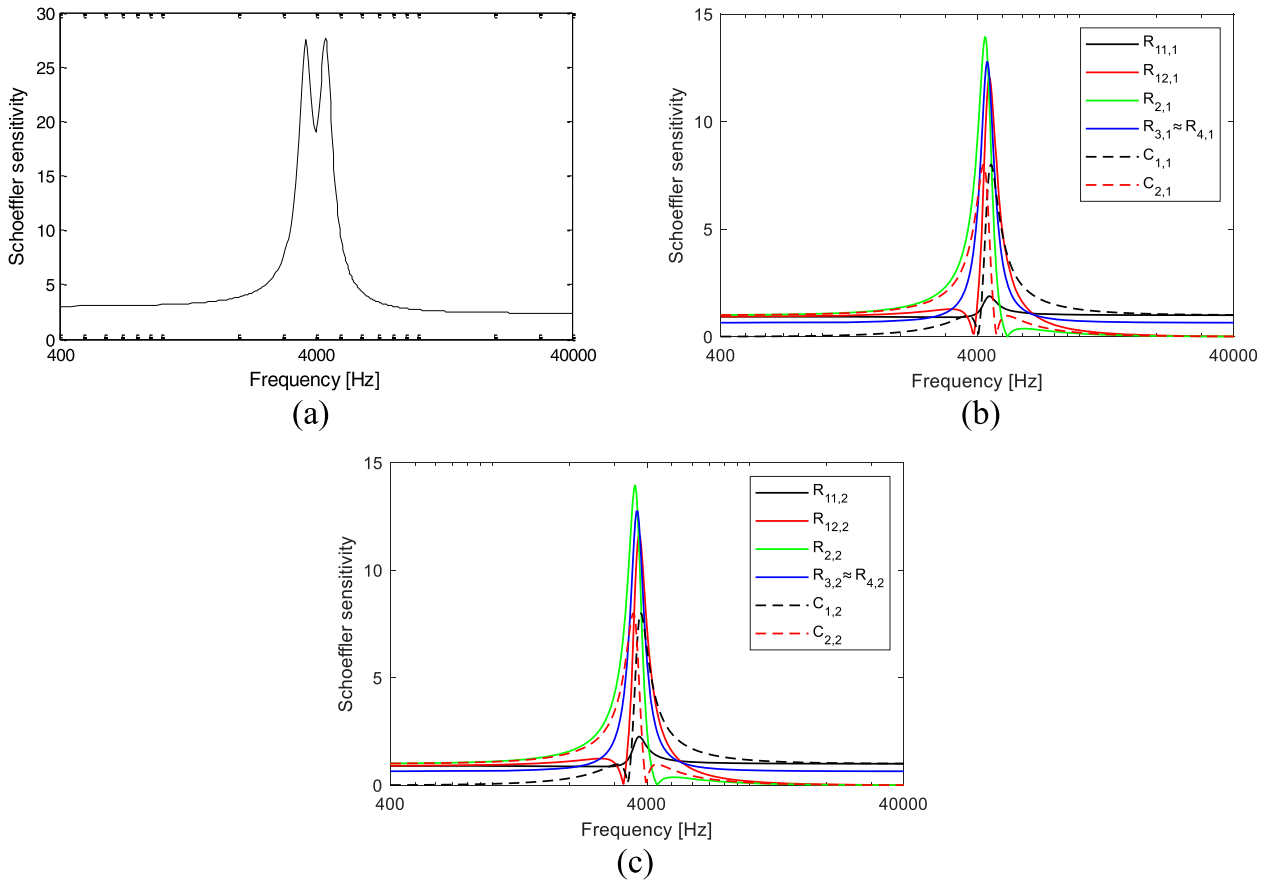


Figure 14. Schoeffler sensitivity of the fourth-order SD band-pass filter. (a) Total Schoeffler sensitivity. The multi-parameter sensitivity calculated in the bandwidth area is $M = 2.3957 \cdot 10^4$. (b) Section 1 Schoeffler sensitivity components. (c) Section 2 Schoeffler sensitivity components.

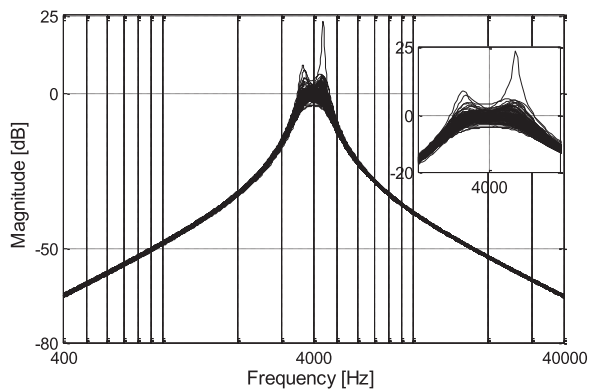


Figure 15. Monte Carlo analysis of the fourth-order SD band-pass filter run over 100 passes with $\pm 1\%$ element tolerance.

influence on the total amount of multi-parameter sensitivity. To prove the results shown in Figure 14, Monte Carlo analysis has been simulated with SPICE. Figure 15 shows Monte Carlo analysis of the fourth-order SD band-pass filter.

We used optimization algorithm given in [7] because we wanted to reduce sensitivity of the filter. For decreasing sensitivity results, all element values were taken from [7], recalculated and tested in MATLAB and

SPICE. Figure 16(a) shows the total sensitivity of the SO filter design, while sensitivity components are specified in Figure 16(b,c) for both sections.

The comparison concludes that the optimized filter has lower multi-parameter sensitivity values. The Monte Carlo analysis of the fourth-order SO band-pass filter is shown in Figure 17.

4.2. Sensitivity in OTA-C filter

Moreover, the Schoeffler sensitivity was calculated using Equation (9) for the fourth-order OTA-C band-pass filter and the results are shown in Figure 18.

The strongest influence on multi-parameter sensitivity of the fourth-order OTA-C band-pass filter in both sections has a sensitivity of elements C_{1i} , C_{2i} , g_{m1i} and g_{m2i} . Figure 19 shows Monte Carlo analysis of the fourth-order SD band-pass filter.

Comparing Figures 15 and 17 with Figure 19, we can conclude that the Monte Carlo analysis in Figure 19 shows much lower spreading in comparison with the others, which is also confirmed with results of the multi-parameter sensitivity.

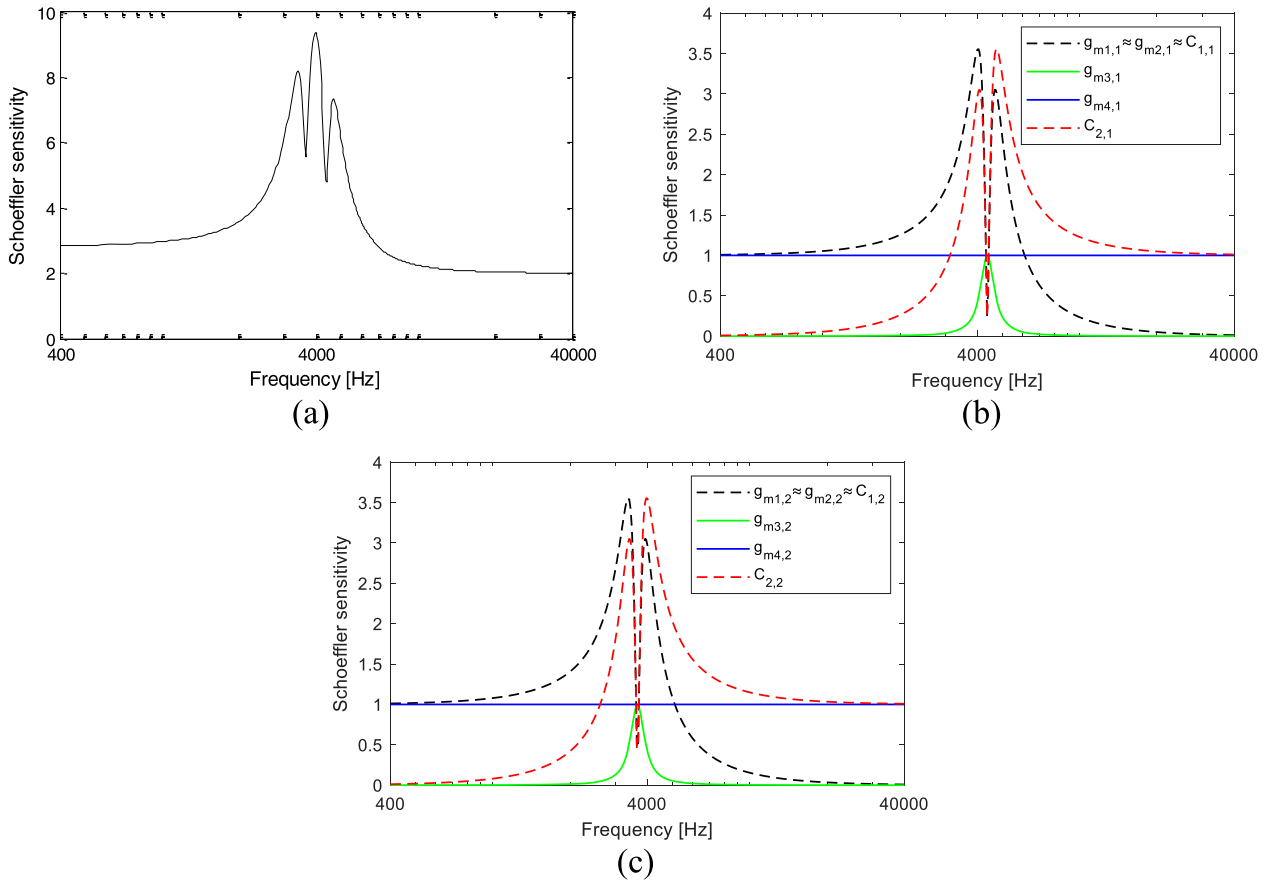


Figure 16. Schoeffler sensitivity of the fourth-order SO band-pass filter. (a) The total Schoeffler sensitivity. The multi-parameter sensitivity calculated in the bandwidth area is $M = 8.2052 \cdot 10^3$. (b) Section 1 Schoeffler sensitivity components. (c) Section 2 Schoeffler sensitivity components.

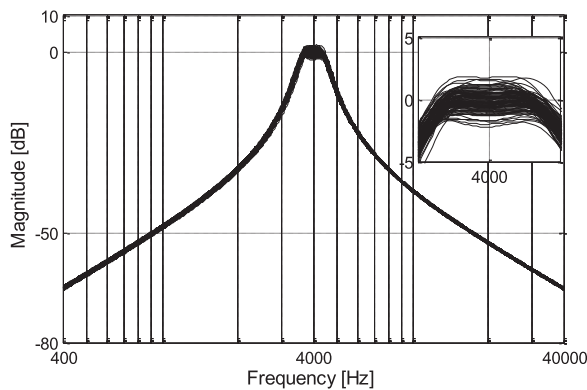


Figure 17. Monte Carlo analysis of the fourth-order SO band-pass filter run over 100 passes with $\pm 1\%$ element tolerance.

4.3. Sensitivity in SC filter

The total sensitivity of each component for both sections is calculated as in [4]. The total sensitivity of the SC filter design is shown in Figure 20(a). Sensitivity components for both sections are shown in Figure 20(b,c).

The strongest influence on multi-parameter sensitivity of the fourth-order SC band-pass filter in both

Table 5. Multi-parameter value comparison.

	SD	SO	OTA-C	SC
M	$2.3957 \cdot 10^4$	$8.2052 \cdot 10^3$	$7.2710 \cdot 10^3$	$6.3969 \cdot 10^3$

sections gives a sensitivity of C_{R2i} , C_{1i} and C_{2i} elements. The Monte Carlo analysis of the fourth-order SC band-pass filter is shown in Figure 21.

In comparison with all other observed filters, the SC filter design in the bandwidth area has the lowest spreading of amplitude response curve in Monte Carlo analysis.

4.4. Sensitivity comparison

If the multi-parameter sensitivity is measured between 3500 and 4500 Hz as the indicator of sensitivity reduction, comparison of sensitivity in all observed designs is given in Table 5. Figure 22 shows the Schoeffler sensitivity of all filter designs studied in this paper.

5. Conclusion

The noise and sensitivity comparison of different filter designs is analysed in this paper. Four different designs were observed. The RMS voltage noise and

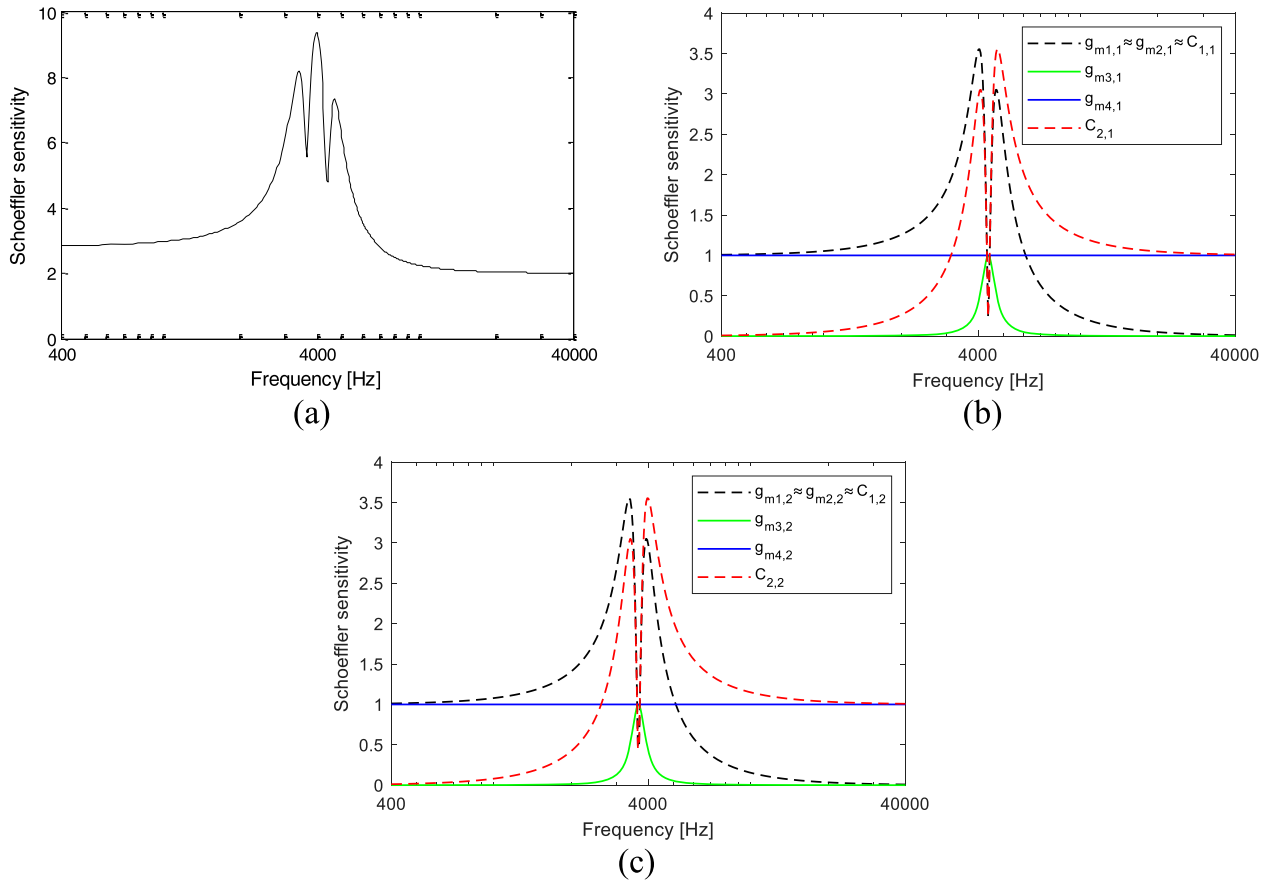


Figure 18. Schoeffler sensitivity of the fourth-order OTA-C band-pass filter. (a) The total Schoeffler sensitivity. The multi-parameter sensitivity calculated in the bandwidth area is $M = 7.2710 \cdot 10^3$. (b) Section 1 Schoeffler sensitivity components. (c) Section 2 Schoeffler sensitivity components.

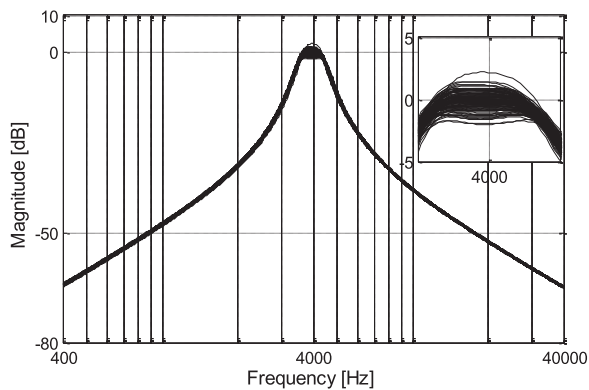


Figure 19. Monte Carlo analysis of the fourth-order OTA-C band-pass filter run over 100 passes with $\pm 1\%$ element tolerance.

multi-parameter sensitivity were used as a measure. The calculation of RMS voltage noise value ($0.1f_c$ to $10f_c$) indicated that the noise improvement for NO design is 2.5 times, OTA-C design 20 times and SC design 10 times, lower in comparison with SD (Šverko et al., 2019). Comparing the RMS voltage noise as a numeric indicator, it can be concluded that the OTA-C filter results in the lowest noise. Moreover, the calculation of the multi-parameter sensitivity between 3.5 and 4.5 kHz showed us that the sensitivity improvement for SO design is 2.9 times, OTA-C design 3.3 times and SC design 3.75 times, lower in comparison with SD. According to that, the best sensitivity reduction is acquired using SC design.

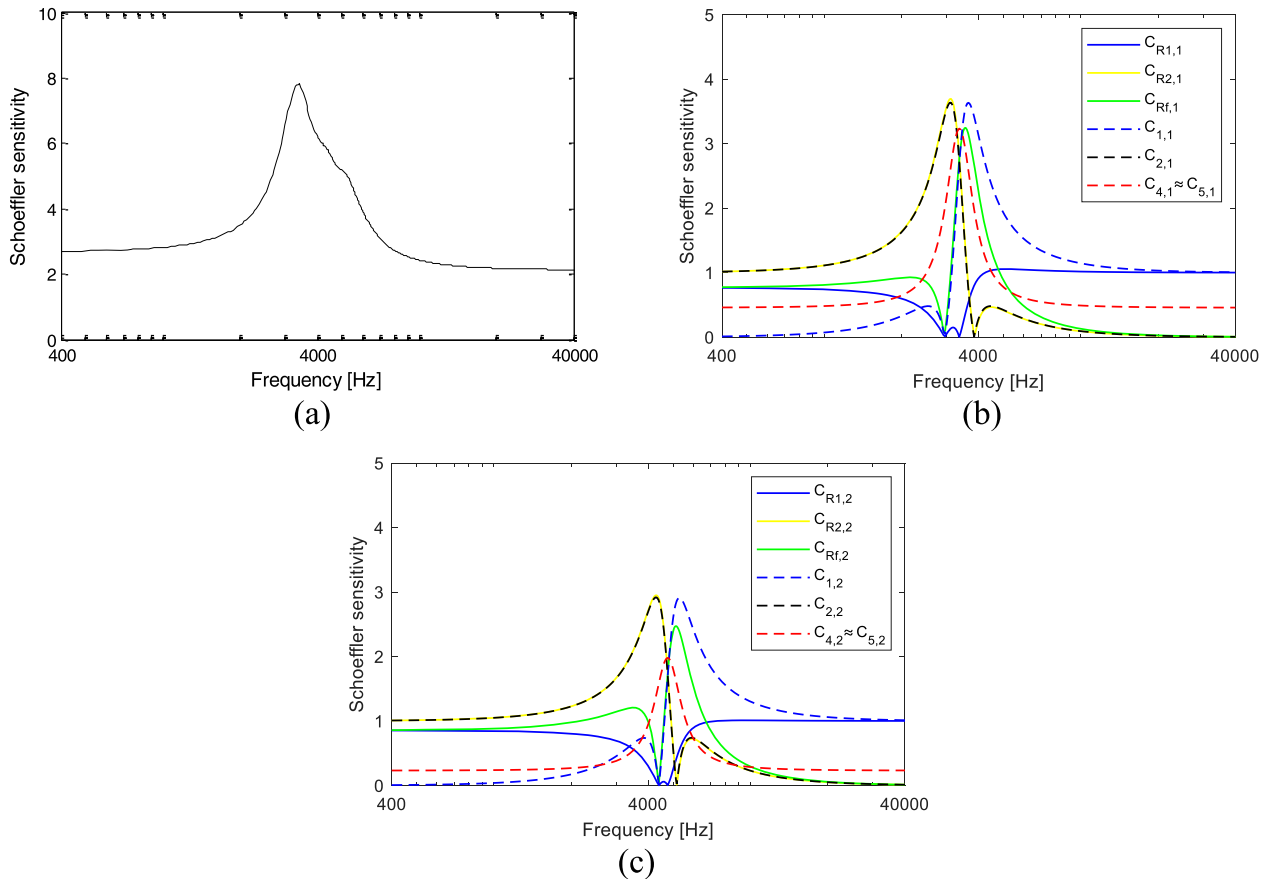


Figure 20. Schoeffler sensitivity of the fourth-order SC band-pass filter. (a) The total Schoeffler sensitivity. The multi-parameter sensitivity calculated in the bandwidth area is $M = 6.3969 \cdot 10^3$. (b) Section 1 Schoeffler sensitivity components. (c) Section 2 Schoeffler sensitivity components.

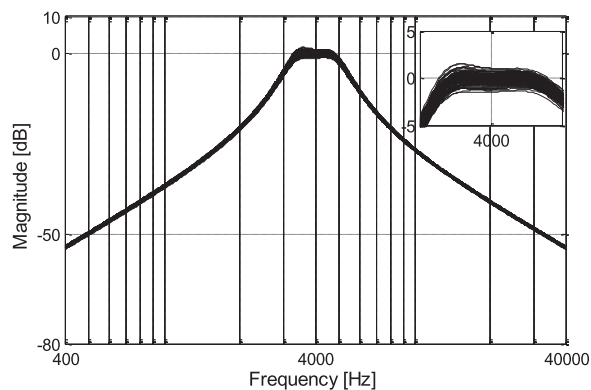


Figure 21. Monte Carlo analysis of the fourth-order SC band-pass filter run over 100 passes with $\pm 1\%$ element tolerance.

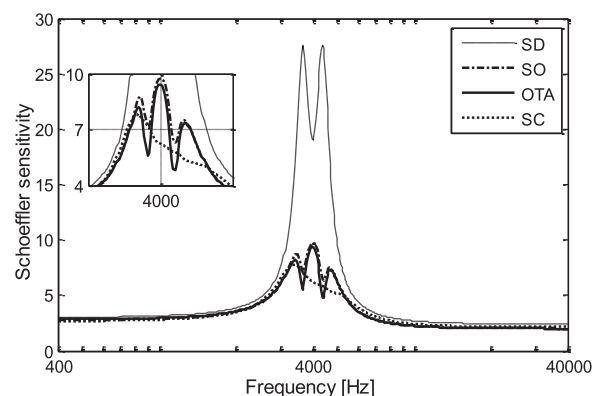


Figure 22. Schoeffler sensitivity for: SD (dashed), SO (dashed-dot), OTA-C (solid), SC (dot-dot).

Disclosure statement

No potential conflict of interest was reported by the author(s).

ORCID

Zoran Šverko  <http://orcid.org/0000-0003-3461-963X>

References

- [1] Serra H. A. D. A. Design of switched-capacitor filters using low gain amplifiers. PhD thesis. Faculdade de Ciências e Tecnologia, 2012.
- [2] Volarić I, Stojković N, Vlahinić S. Noise improvement using SC filters. 2015 38th International Convention on Information and Communication Technology, Electronics and Microelectronics (MIPRO), IEEE.; 2015: 121–126.
- [3] Volarić I, Stojković N, Vlahinić S. Noise and sensitivity improvement using SC filters. *Automatika: Časopis za Automatiku, Mjerenje, Elektroniku, Računarstvo i Komunikacije*. 2015;56(4):491–498.
- [4] Šverko, Z, Stojković, N, Vlahinić, S, et al. Noise improvement for different BP filter designs. In: 2019 42nd International Convention on Information and Communication Technology, Electronics and Microelectronics (MIPRO), IEEE.; 2019: 122–127.

- [5] Jurisic D, Moschytz GS. Low-noise and low-sensitivity filters using current-mode coupled biquads. *Int J Circuit Theory Appl* 2019; 47(11): 1713–1735.
- [6] Jurisic D, Moschytz GS. Minimum sensitivity coupled resonators and biquads. *Int J Circuit Theory Appl*. 2019;47(9):1383–1401.
- [7] Stojković N, Kamenar E, Šverko M. Optimized second- and fourth-order LP and BP filters. *Automatika*. 2011;52(2):158–168.
- [8] Mu H, Zhu Y, Sun Y. Design for testability of high-order OTA-C filters. *Int J Circuit Theory Appl*. 2016;44(10):1859–1873.
- [9] Wadhwa N, Bahubalindrani PG, Chapagai K, et al. Sixth-order differential sallen-and-Key switched capacitor LPF using a-IGZO TFTs. *Int J Circuit Theory Appl*. 2019;47(1):32–42.
- [10] Shi G, Zhang A, Gu Y. A comparative study on using linear programming and simulated annealing in the optimal realization of a SC filter. *Int J Circuit Theory Appl*. 2017;45(12):2134–2148.
- [11] Chen WK. *The circuits and filters handbook*, 2nd ed. CRC Press, London. 2003.
- [12] Im S, Park SG. Thermal noise analysis of switched-capacitor integrators with correlated double sampling. *Int J Circuit Theory Appl* 2016; 44(12): 2101–2113.
- [13] Fischer JH. Noise sources and calculation techniques for switched capacitor filters. *IEEE J Solid-State Circuits*. 1982;17(4):742–752.
- [14] Schoeffler J. The synthesis of minimum sensitivity networks. *IEEE Trans Circuit Theory*. 1964;11(2):271–276.